surfaces

MDPI

Article

Superhydrophilic Titania Coatings on Glass Substrates via the Hydrosol Approach

George V. Theodorakopoulos [1,*], Michalis K. Arfanis [1], Nafsika Mouti [2], Andreas Kaidatzis [1], Christian Mitterer [2], Konstantinos Giannakopoulos [1] and Polycarpos Falaras [1,*]

[1] Institute of Nanoscience and Nanotechnology, National Centre for Scientific Research (NCSR) "Demokritos", Agia Paraskevi, 15341 Athens, Greece; m.arfanis@inn.demokritos.gr (M.K.A.); a.kaidatzis@inn.demokritos.gr (A.K.); k.giannakopoulos@inn.demokritos.gr (K.G.)

[2] Department of Materials Science, Montanuniversität Leoben, Franz-Josef-Straße 18, 8700 Leoben, Austria; nafsika-maria.mouti@unileoben.ac.at (N.M.); mitterer@unileoben.ac.at (C.M.)

* Correspondence: g.theodorakopoulos@inn.demokritos.gr (G.V.T.); p.falaras@inn.demokritos.gr (P.F.); Tel.: +30-210-650-3977 (G.V.T.); +30-210-650-3644 (P.F.)

Abstract: This study presents a comprehensive investigation into the synthesis and characterization of TiO_2 coatings on glass substrates, focusing on the development of superhydrophilic, self-cleaning titania coatings using the hydrosol approach. Stringent cleaning protocols were accurately followed to ensure the pristine condition of glass surfaces prior to deposition. Various organic precursor solutions were precisely prepared and applied to the glass substrate via dip-coating, followed by subsequent thermal treatment. A range of characterization techniques, including Raman spectroscopy, UV/Vis spectroscopy, scanning and atomic force microscopy, X-ray photoelectron spectroscopy, and contact angle measurements, were employed to assess the properties of the coatings. The results revealed that the samples were influenced by precursor concentration and withdrawal rate, with slow speed leading to minimal alteration of transmittance. The coatings show superhydrophilic properties, as evidenced by contact angle values below 3 degrees for the thinnest films. Their thickness is approximately 13 nm with very low roughness, indicative of a smooth and uniform surface. Optimization of the deposition conditions permits the fabrication of uniform and transparent TiO_2 coatings on glass substrates, offering promising opportunities for the practical use of photoinduced self-cleaning surfaces in real-life applications. Finally, a cost analysis of scaling up the coating and mirror fabrication processes confirmed the economic feasibility of this approach for concentrated solar power (CSP) applications.

Keywords: titania coatings; dip-coating; hydrosol method; superhydrophilic; self-cleaning; optical properties

Academic Editors: Jaeho Kim and Susumu Yonezawa

Received: 30 November 2024
Revised: 27 December 2024
Accepted: 3 January 2025
Published: 6 January 2025

Citation: Theodorakopoulos, G.V.; Arfanis, M.K.; Mouti, N.; Kaidatzis, A.; Mitterer, C.; Giannakopoulos, K.; Falaras, P. Superhydrophilic Titania Coatings on Glass Substrates via the Hydrosol Approach. *Surfaces* **2025**, *8*, 5. https://doi.org/10.3390/surfaces8010005

1. Introduction

Titanium dioxide (TiO_2), commonly known as titania, is a widely studied material due to its exceptional optical, chemical, and photocatalytic properties [1,2]. These characteristics make it a highly versatile material in various applications, including solar cells [3,4], self-cleaning surfaces [1,5,6], and environmental purification systems [7–10]. TiO_2 is a widely studied material for developing superhydrophilic coatings due to its photocatalytic properties, chemical stability, and non-toxicity. When engineered to be superhydrophilic, titania surfaces exhibit unique characteristics that make them highly suitable for applications requiring antireflective and self-cleaning properties. Recent advancements have focused on enhancing its antireflective and superhydrophilic properties, which are crucial for boosting the efficiency and functionality of devices that utilize titania [11,12].

Superhydrophilic surfaces are characterized by extremely low contact angles, nearly to a zero apparent contact angle (typically below 5 degrees) [13], allowing water droplets to spread out completely and facilitating self-cleaning properties. This property ensures water disperses uniformly over the surface, forming a continuous, thin film that effectively removes contaminants and enhances the self-cleaning effect. The superhydrophilic nature of titania coatings primarily arises from their high surface energy and porous structure, which promotes strong interactions with water molecules. The formation of TiO_2 in the anatase phase has been associated with enhanced wettability due to the high density of hydroxyl groups on the surface, which facilitates hydrogen bonding with water [14,15]. This phenomenon can be further enhanced through post-deposition treatments such as UV radiation, which can increase the surface hydroxyl density and activate the photocatalytic properties of the TiO_2 layer [16,17]. The superhydrophilic nature of the coatings allows rain or water to easily wash away dust and contaminants, maintaining their transparency and performance over time. Additionally, the photocatalytic properties of TiO_2 contribute to self-cleaning capabilities. When exposed to UV light, TiO_2 generates reactive oxygen species that break down organic contaminants on the surface. This photocatalytic effect, combined with the superhydrophilic characteristic [18,19], forms a thin water film that rinses away dust, dirt, and organic contaminants, keeping surfaces clean without requiring harsh chemicals [20].

Titania-based antireflective coatings are designed to minimize light reflection and enhance light transmission through a surface [1,21], which is particularly beneficial in solar energy applications, where maximizing light absorption is essential for improving energy conversion efficiency. The nanostructuring of TiO_2 enables a gradual refractive index transition, significantly reducing surface reflections [11]. Additionally, these coatings can be engineered to possess self-cleaning properties, further enhancing their durability and practicality in real-world applications. The antireflective properties of superhydrophilic titania are closely related to its surface texture and the refractive index gradient formed by the nanostructured surface. The controlled fabrication of titania's surface morphology can minimize reflection across a broad spectrum of light wavelengths, thereby increasing transparency. This approach has been shown to enhance light transmission in the visible range [22], making it ideal for photovoltaic cells and optical lenses. By decreasing the surface reflectivity, these coatings improve light transmission, and, in turn, the efficiency of both photovoltaic cells and optical devices.

Various techniques have been employed to develop titania coatings and thin films on various substrates such as chemical vapor deposition [23], RF/DC magnetron sputtering deposition [24], electrophoretic deposition [25], pulsed laser ablation/deposition [26], anodic oxidation [8,27], ion-assisted deposition [28], vacuum arc plasma evaporation [29], screen-printing [30], and sol-gel methods [8,31]. The sol-gel method is a widely used technique for developing homogeneous TiO_2 films through the hydrolysis and condensation of titanium alkoxide precursors. Thin films can be deposited onto a substrate using spin-coating [32] or dip-coating [31,33] techniques. Dip-coating is a simple and cost-effective method with significant advantages including the ease of anchoring TiO_2 onto substrates with complex shapes or large surface areas [31].

In this study, the effect of various deposition parameters on the morphological, structural, and optical properties of TiO_2 thin films deposited on glass tiles using the dip-coating technique has been explored. This investigation employed Raman spectroscopy, UV/Vis spectroscopy, scanning electron microscopy (SEM), atomic force microscopy (AFM), X-ray photoelectron microscopy (XPS), and contact angle measurements. Additionally, the long-term stability of the films and a cost analysis for scaling up the process for CSP mirror fabrication were examined.

2. Materials and Methods

2.1. Materials Synthesis

To deposit TiO_2 coatings onto commercial glass tiles, allowing for the subsequent development of an Ag-based mirror on the backside via chemical techniques, it was essential to ensure that the glass surface was free of any dirt. In order to prevent dirt contamination, which could affect the quality and physicochemical properties of the film, specific cleaning protocols were followed. In short, pre-cut 4 × 4 cm glass tiles were cleaned through consecutive sonication in ultrapure water (Milli-Q, 18 MΩ·cm) with 2% *v*/*v* Hellmanex, acetone, and isopropanol (IPA) for 15 min [34].

For the deposition of the TiO_2 coatings, an organic precursor sol was prepared consisting of 14 g of non-ionic surfactant Triton X-100, 76 mL of absolute ethanol, 13.6 mL of glacial acetic acid (AcOH), and 7.2 mL of titanium isopropoxide (TTIP) [35]. Additionally, the TTIP concentration was diluted to half, a quarter, or an eighth by adding the appropriate amount of absolute ethanol, and these final solutions were used for further deposition cycles. The deposition of titania onto the glass substrates for only one dip was carried out using an Ossila dip-coater. The withdrawal speed was a key factor in the deposition process, ranging from low (0.5 mm/s) to moderate (5 mm/s) and high speed (50 mm/s). Finally, thermal treatment was applied at 550 °C for 1 h, transforming the aforementioned coatings into smooth, compact, and crystalline titania layers of low thickness, suitable for photo-induced applications [36]. The specific deposition parameters for twelve different coating samples are detailed in Table 1.

Table 1. Deposition conditions with the organic sol.

Sample	TTIP Concentration	Withdrawal Speed (mm/s)
Co-l	Co	0.5
Co-m	Co	5
Co-h	Co	50
Co/2-l	Co/2	0.5
Co/2-m	Co/2	5
Co/2-h	Co/2	50
Co/4-l	Co/4	0.5
Co/4-m	Co/4	5
Co/4-h	Co/4	50
Co/8-l	Co/8	0.5
Co/8-m	Co/8	5
Co/8-h	Co/8	50

2.2. Characterization Techniques

To develop TiO_2 films using the hydrosol approach, the deposition parameters were thoroughly examined, including the solvent and precursor, substrate type (mirror and glass), and withdrawal speed. To achieve these objectives, three main characterization techniques were utilized: vibrational Raman spectroscopy, UV/Vis spectroscopy, and contact angle measurements. Raman measurements were performed with a Renishaw In-Via Reflex dispersive micro-Raman spectrometer (Renishaw, Wotton-under-Edge, UK) with <2 cm^{-1} resolution and a diode laser, emitting at λ = 514.4 nm, as the excitation source. A ×100 objective lens on a Leica DMLM microscope (Leica Microsystems GmbH, Wetzlar, Germany) was used to focus the laser beam to a sizeable spot of 1 μm in diameter on the samples' surface. Rayleigh scattering was rejected with 110 cm^{-1} cutoff dielectric edge filters, and analysis of the scattered beam was performed on a 250 mm focal length

spectrometer along with suitable diffraction gratings (1800 lines/mm) and a high sensitivity CCD detector.

The optical properties of the samples were analyzed using a Hitachi 3010 UV/Vis spectrophotometer (Hitachi Ltd., Tokyo, Japan), equipped with a 60 mm diameter integrating sphere and $BaSO_4$ as a reference. The films' morphology was examined using a FEI Quanta-Inspect scanning electron microscope (FEI Company, Eindhoven, The Netherlands), which operated with a tungsten filament at 25 kV, along with a Bruker Dimension Icon atomic force microscope AFM (Bruker Corporation, Billerica, MA, USA). AFM imaging has been performed in non-contact mode, using commercially available PPP-NCH probes from Nanosensors. The film thickness was determined using a J.A. Woollam M2000F rotating compensator ellipsometer (RCE™, J.A. Woollam Co., Inc., Lincoln, NE, USA) operated at an incidence angle of 75.14°. The elemental surface analysis of the coatings was conducted using an energy dispersive spectrometer—EDS (Oxford Instruments, Wycombe, UK) coupled with the SEM, and X-ray photoelectron spectroscopy XPS (Nesa GS Surface Analysis System, Thermoscientific, Waltham, MA, USA). For XPS, a monochromatic, microfocused, low-power Al Kα X-ray (1486.7 eV) beam focused to a spot size of 300 μm was used. XPS wide range survey spectra were acquired with a pass energy of 200.0 eV and a step size of 1.0 eV, while high-resolution spectra were measured using a pass energy of 50.0 eV and a step size of 0.1 eV. The binding energy scale was calibrated to the C–C 1s signal at 284.8 eV. Multiple scans were performed for accuracy, and the Ti 2p and O 1s spectra showed distinct peaks at binding energies of 458.93 eV (Ti 2p) and 530.85 eV (O 1s), confirming the expected chemical states. The hydrophilicity of the TiO_2 thin films was evaluated using a contact angle meter (CAM 100, KSV Instruments Ltd., Helsinki, Finland) equipped with the appropriate software. Two series of experiments were performed: initially, contact angles (CA) were measured immediately on the prepared samples (these measurements are referred to as "standard method"). Afterwards, the samples were irradiated with UV-A light (intensity ~2.6 mW·cm^{-2}) for five minutes, after which CA measurements were repeated to assess photo-induced hydrophilicity. In most cases, the measurements were repeated three times due to limitations in the available sample surface, and the mean values are presented.

3. Results

3.1. Physicochemical Characterization

The following section presents the physicochemical properties of the titania films deposited onto glass slides using the organic precursor solutions. Starting with the UV/Vis spectroscopy data shown in Figure 1a–d, it was observed that the transmittance decrease was more intense for concentrated precursor solutions (compared to the reference glass slide). Moreover, the fast deposition speed (50 mm/s) negatively affected the optical properties of the samples, while the slowest speed of 0.5 mm/s did not alter significantly the transmittance. This trend was particularly evident in the case of the precursor solution Co, where the transmittance reduction reached approximately 10% for the quickest speed, about 4.5% for the intermediate speed, and below 0.7% for the slowest deposition. The negative impact of faster deposition speeds (50 mm/s) on optical properties is likely due to insufficient time for uniform film formation, leading to a thicker or less homogeneous coating, which increases light scattering and absorption, thereby reducing transmittance. In contrast, slower speeds (0.5 mm/s) allow for more controlled deposition, resulting in a thinner, smoother, and more uniform film that better maintains the transparency of the glass. This behavior is particularly noticeable with the precursor solution Co, where faster deposition causes a greater reduction in transmittance, while slower speeds produce minimal changes, suggesting improved film quality at lower speeds. Interestingly, the induced transmittance did not decrease more than 1% using the diluted precursor solutions,

which is very promising for integrating self-cleaning materials with CSP collectors. The only exception was the sample Co/2-h, suggesting that the very high speed did not yield TiO_2 films of high quality. By taking into account the macroscopic homogeneity of the films, the most promising coatings were derived from conditions Co/4 and Co/8 at deposition speeds of 0.5 and 5 mm/s.

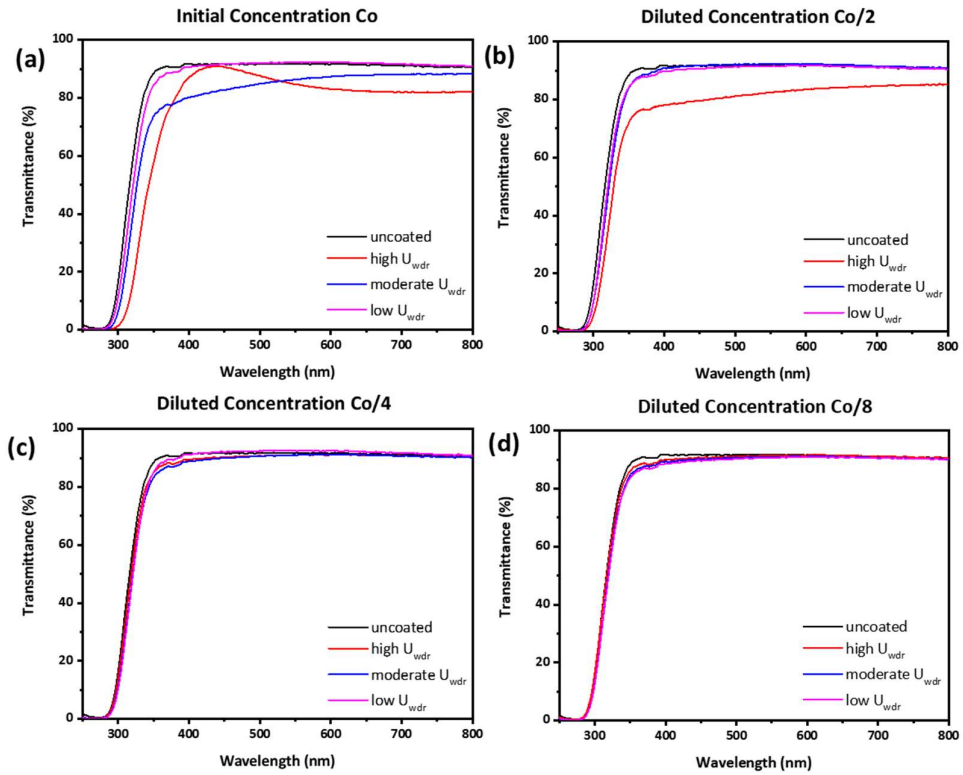

Figure 1. Transmittance spectra of glass slides after TiO_2 deposition using different TTIP concentrations: (**a**) Co; (**b**) Co/2; (**c**) Co/4; and (**d**) Co/8 and for various withdrawal speeds (0.5 to 50 mm/s).

For SEM analysis (Figure 2), a reference glass slide and the samples Co-m, Co/2-m, Co/4-m, and Co/8-m were selected as the most suitable materials. The surface of the reference glass slide appeared clean, smooth, and homogenous, with no detectable roughness. In contrast, upon the deposition of the Co-m coating, the surface was totally covered by a dense layer of TiO_2 nanoparticulate aggregates. When the TTIP concentration was decreased (Co/2-m), the resulting films displayed fewer aggregates, which were more sparsely dispersed across the surface. The aggregate density decreased further with solution Co/4-m, although their size slightly increased. In sample Co/8-m, the aggregates almost disappeared, and only isolated grains were visible across the tested area. These observations help to explain the aforementioned differences in optical properties: the concentrated precursor solution (Co-m) formed an extensive network of TiO_2 aggregates that blocked incident light, reducing transmittance. In contrast, the more diluted solutions led to dispersed TiO_2 building blocks on the glass surface, allowing for better light penetration and thus higher transmittance. As the dilution increased, the TiO_2 coverage became less dense, enhancing optical transparency while still maintaining the stability of the film structure.

Table 2 presents data on the thickness of TiO_2 coatings deposited on glass tiles, as measured by an ellipsometer, revealing a significant variation in thickness values ranging from 11 nm to 121 nm. The observed differences in film thickness are clearly influenced by the TTIP precursor concentration and withdrawal speed during the deposition process. As

the TTIP concentration decreases (e.g., Co-m, Co/2-m, Co/4-m, Co/8-m), the film thickness at the same withdrawal speed decreases significantly. For instance, the Co-m sample has a thickness of 50 nm, while Co/2-m and Co/4-m exhibit progressively thinner coatings of 23 nm and 11 nm, respectively.

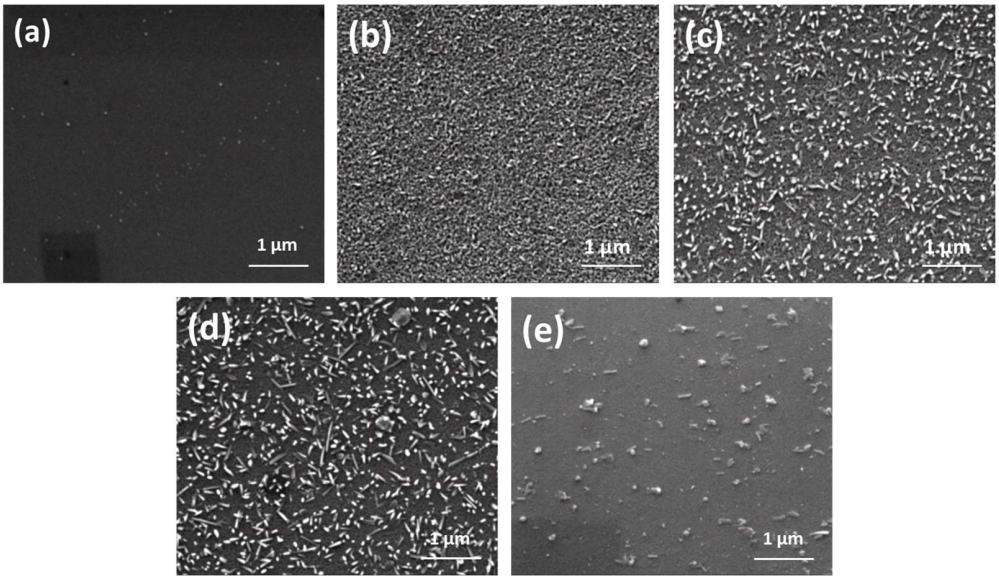

Figure 2. SEM images of a reference glass slide (**a**); and TiO_2 coatings prepared using sols with TTIP concentration of Co (**b**); Co/2 (**c**); Co/4 (**d**); and Co/8 (**e**), for a withdrawal speed of 5 mm/s.

Table 2. Film thickness of TiO_2 coatings on glass tiles measured by ellipsometry.

Sample	Thickness (nm)
Co-m	50
Co/2-m	23
Co/4-l	13
Co/4-m	11
Co/4-h	121
Co/8-m	out of range

The above behavior highlights the reduced availability of titania particles in the coating solution, leading to thinner films on the glass surface. Furthermore, the Co/8-m sample was classified as out of range, likely due to an extremely thin or non-uniform film that the ellipsometer could not measure accurately. This trend, illustrated in Figure 3, indicates the critical role of precursor concentration in controlling film thickness during deposition. The strong linear correlation ($R^2 = 0.998$) between TiO_2 film thickness and TTIP precursor concentration at a withdrawal speed of 5 mm/s demonstrates that film thickness is directly proportional to precursor concentration. This relationship confirms TTIP concentration as the dominant factor in controlling the film thickness, enabling precise tailoring of film properties by adjusting the precursor composition.

The withdrawal speed also significantly affects film thickness, as demonstrated in the Co/4 group. A low withdrawal speed produces a thinner coating (13 nm), while a high one results in a much thicker film (121 nm). Higher speeds likely lead to thicker films by rapidly removing the substrate from the coating solution, capturing a larger liquid volume that solidifies upon drying. Overall, these results highlight the critical roles of precursor concentration and withdrawal speed in controlling film thickness offering valuable insights for optimizing the coating process to achieve desired properties such as uniformity and functional performance.

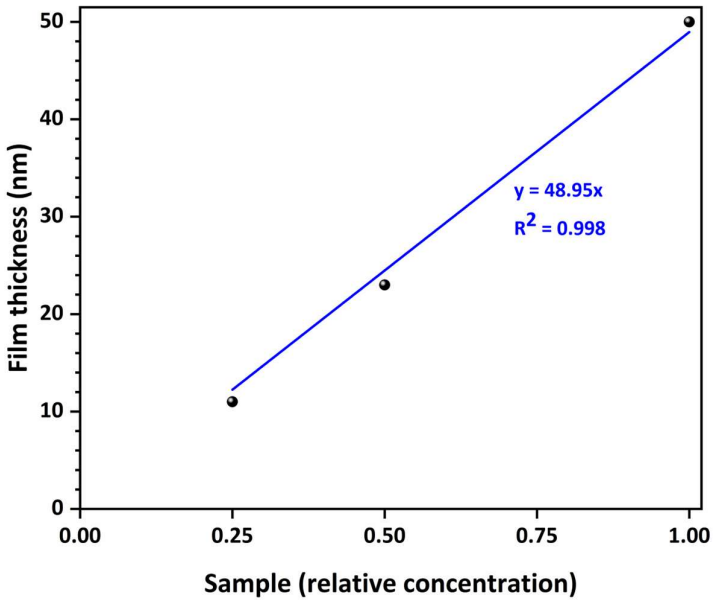

Figure 3. Dependence of film thickness on TTIP precursor concentration (Co = 1× precursor concentration, Co/2 = 1/2×, Co/4 = 1/4×) at medium withdrawal speed (5 mm/s).

XRD was subsequently utilized to analyze the crystallinity of the coatings. Based on the UV/Vis results, Co-l and Co/8-h samples were selected as representative thick and thin samples, respectively, since they were prepared under different deposition conditions, making them appropriate for XRD analysis. The diffraction patterns revealed no characteristic peaks for either anatase and/or rutile phases. This suggests that the thickness of the films and/or the final content of crystalline TiO_2 in both samples was too low and well distributed across the glass substrate, preventing the detection of distinct phases. This implies that, under the specific conditions, crystallization may not fully occur, or the resulting crystalline domains may be too small to be observed.

On the other hand, Raman spectroscopy was able to detect surface vibrations, despite the material content being low and dispersed across a substrate. As expected, the main vibration mode of anatase, observed at 143 cm^{-1} in Figure 4, was identified, confirming that the films' chemical bond formation and probably also crystallization was successfully achieved during the annealing process [8]. A major advantage of Raman spectroscopy is its high sensitivity, allowing it to detect vibrational modes even in thin films or when the material is present in small quantities. This demonstrates that, despite the limited material and its dispersion, Raman spectroscopy can effectively confirm structural changes like chemical bond formation and crystallization, providing important insights into the phase composition at the surface level.

X-ray photoelectron spectroscopy (XPS) revealed that the surface chemistry of the fabricated coatings matches with substoichiometric titanium oxides, possibly titanium oxyhydroxide ($TiO(OH)_2$). In particular, the high-resolution XPS spectrum of the Ti 2p region (Figure 5a) displays distinct peaks for Ti $2p_{3/2}$ and Ti $2p_{1/2}$, centered at binding energies of 457.7 and 463.4 eV, respectively, which are assigned as Ti^{3+} species [37]. Additionally, the O 1s photoelectron spectrum was deconvoluted into two components: one at 529.1 eV corresponding to lattice oxygen in Ti-O bonds, and another at 530.6 eV corresponding to Ti-OH groups, which are indicative of either defective oxides or adsorbed OH^- on the oxide surface (Figure 5b) [38]. These findings imply that the synthesized TiO_2 film has the ability to chemisorb water molecules, forming an extremely thin water layer on the surface. This characteristic indicates that the coating is likely to exhibit superhydrophilic

properties [20], enhancing its potential application in areas such as self-cleaning surfaces and photocatalysis.

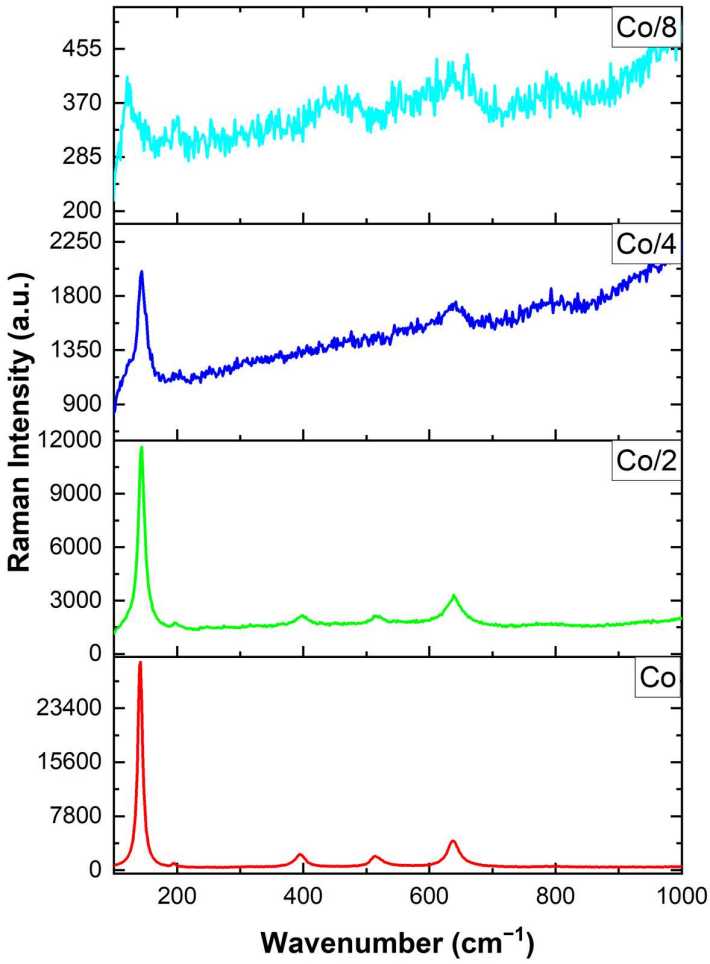

Figure 4. Representative Raman spectra for sol-gel samples.

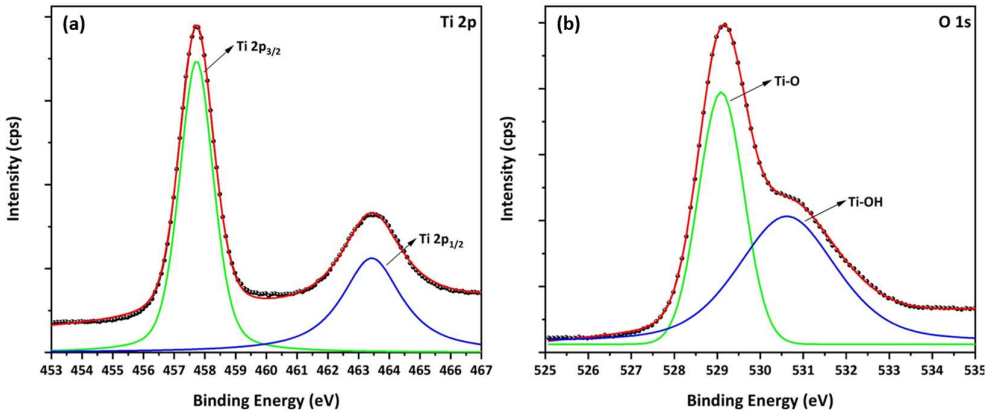

Figure 5. High-resolution XPS spectra of the Co/4 sample in the Ti 2p (**a**); and O 1s region (**b**).

3.2. Surface Wettability

Contact angle measurements were performed for all the TiO_2 coatings to assess their wettability. The obtained results indicated that all the samples exhibited significantly improved wetting properties compared to the reference glass slide (Figure 6 and Table 3). This enhancement suggests that the surface properties of the TiO_2 coatings have been modified to increase their hydrophilicity, enabling water droplets to spread more easily across the surface. A low contact angle reflects a stronger interaction between the surface

and the liquid, signifying improved wetting behavior. Such characteristics are highly beneficial for applications like self-cleaning surfaces, photocatalysis, and anti-fogging coatings. The comparison with the reference glass slide underscores the superior ability of the TiO_2 coatings to promote surface wetting, a crucial factor in optimizing their functional performance across a wide range of technological applications.

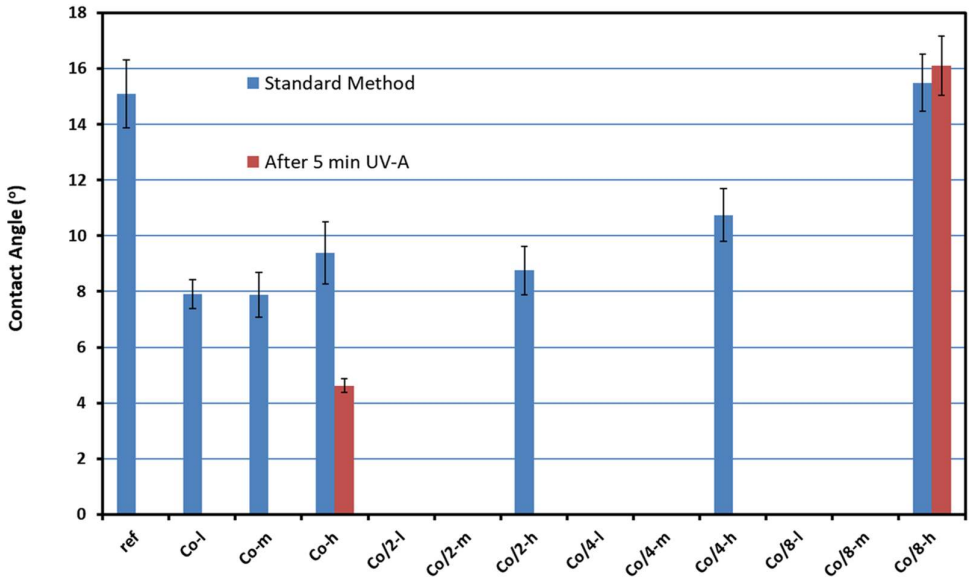

Figure 6. Contact angle measurements of the coated samples produced from organic sols with varying TTIP concentration and withdrawal speeds. The software of the instrument is unable to accurately calculate angles below 3°.

Table 3. Contact angle (CA) measurements of TiO_2 coatings prepared under varying deposition conditions (TTIP concentration and withdrawal speed).

Sample	Standard Method	After 5 min UV-A
	CA (°)	
reference	15.09 ± 1.21	-
Co-l	7.92 ± 0.52	0
Co-m	7.89 ± 0.81	0
Co-h	9.39 ± 1.12	4.63 ± 0.26
Co/2-l	<3	<3
Co/2-m	<3	<3
Co/2-h	8.76 ± 0.87	<3
Co/4-l	<3	<3
Co/4-m	<3	<3
Co/4-h	10.75 ± 0.94	<3
Co/8-l	<3	<3
Co/8-m	<3	<3
Co/8-h	15.49 ± 1.03	16.10 ± 1.06

Interestingly, many samples demonstrated remarkable performance, exhibiting contact angles that approached zero (Figure 7). Practically, the software of the instrument is unable to accurately calculate angles below 3°. The deposition conditions along with the resulting film thickness played a significant role in enhancing the super-hydrophilic properties of these films. Specifically, the samples that displayed near-zero contact angles were mainly those with the most uniform structures, fabricated using diluted Co/4 solutions and moderate withdrawal speeds during the coating process. This suggests that both the

preparation methods and the specific parameters utilized during deposition are crucial for achieving optimal hydrophilic properties in the resulting films.

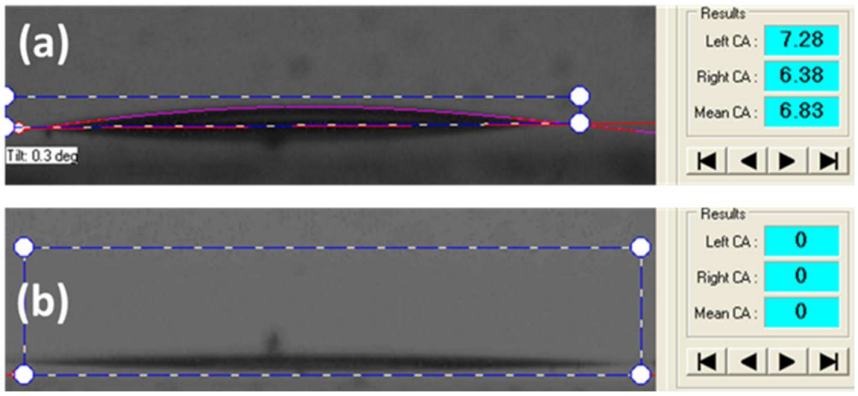

Figure 7. Indicative contact angle images of a super-hydrophilic sample: within detection limits (sample Co-m) (**a**); below the detection limits of the software (sample Co/4-m) (**b**).

The UV-A light treatment was performed exclusively for samples with measurable contact angles, and the subsequent analysis demonstrated that these samples exhibited super-hydrophilic properties after illumination, resulting in zero contact angle values. No improvement in wettability was observed for the Co/8-h samples (see Figure 6 and Table 3), indicating that their wetting characteristics remained unchanged. In combination with the previous results, it is possible that the Co/8 solution, when applied at a withdrawal speed of 50 mm/s, does not provide sufficient coverage on the glass substrate, allowing the inherent hydrophilic properties of the glass slide to dominate.

In summary, the physicochemical analysis of the coated glass slides indicates that the concentration of the precursor solution and the withdrawal speed are critical factors for achieving uniform and transparent superhydrophilic TiO_2 coatings. Focusing on the precursor organic solutions, the samples exhibiting the required optimal optical properties were derived from the diluted Co/4 solution, while the withdrawal rate of 0.5 mm/s seems to be the ideal deposition speed in terms of macroscopic surface homogeneity.

3.3. AFM Analysis

AFM analysis provides valuable insights into the surface morphology of the TiO_2 coatings on the glass substrate. The AFM images in Figure 8a depict the bare glass substrate, showing a relatively smooth surface with minimal height variation, indicating that the glass itself contributes little to surface roughness. However, the Co/4 sample in Figure 8b reveals noticeably different surface features depending on the withdrawal rates used during the coating process. At higher withdrawal rates, the TiO_2 coating develops more pronounced surface features, with larger particles or agglomerates scattered across the surface. In contrast, lower withdrawal rates result in a smoother, more uniform surface, indicating a finer deposition of the TiO_2 coating.

The height profiles in Figure 8c, derived from AFM images, provide a clear representation of the surface roughness and topography of TiO_2 coatings on glass substrate prepared at different withdrawal rates. The high-rate sample shows the most significant surface roughness, with sharp peaks reaching up to 160 nm, while the medium- and low-rate coatings exhibit progressively lower roughness. The low-rate sample exhibits the smallest height variations, with roughness reaching up to 40 nm, indicating a smoother and more uniform surface, close to the flatness of the bare glass substrate. A similar behavior is observed in the medium-rate sample. On the other hand, as the withdrawal rate increases, the surface roughness becomes more pronounced, with larger surface features and increased

particle aggregation. This trend suggests that faster withdrawal rates lead to less controlled deposition, resulting in a rougher, less uniform coating. In contrast, lower withdrawal rates allow for more controlled and uniform film formation. These findings underscore the importance of controlling withdrawal rates to achieve the desired surface texture and uniformity, which is crucial for applications like optics, photocatalysis, or protective coatings, where surface characteristics are critical.

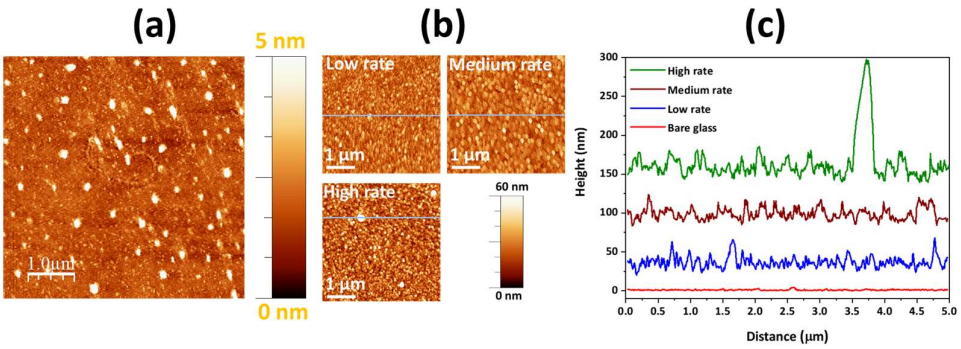

Figure 8. 2D AFM images of the (**a**) bare substrate, and (**b**) Co/4 sample; (**c**) corresponding height profiles. The vertical scale is 5 nm in (**a**) and 60 nm in (**b**).

The root mean square (RMS) roughness values estimated from the AFM image analysis for the Co/4 sample, in comparison to the bare glass substrate, are listed in Table 4. The significant increase in RMS roughness from 0.7 nm for the bare glass substrate to 10 nm for the Co/4-h sample indicates that the withdrawal rate during the coating process greatly impacts the surface texture of the TiO_2 coating. As the withdrawal rate increases from low to high, the surface roughness progressively grows, peaking at the highest withdrawal rate. This trend suggests that a faster withdrawal leads to a less uniform deposition, possibly due to more rapid solvent evaporation or uneven accumulation of TiO_2 particles, resulting in a rougher film surface. Variations in surface roughness can affect the material's optical, functional, and adhesive properties, which are crucial for the applications being studied. Furthermore, the findings highlight the importance of controlling the withdrawal rate during deposition to optimize surface characteristics. While a lower withdrawal rate yields a relatively smooth film, higher rates may lead to increased roughness, potentially impacting performance. Thus, controlling the withdrawal rate is essential for tailoring the surface properties of TiO_2 coatings to meet specific application requirements. In this context, the Co/4-l sample stands out as the best and most promising candidate for antireflective and self-cleaning applications. Its moderate roughness optimizes light scattering for enhanced antireflective properties, while also maintaining clarity and improving self-cleaning effectiveness through balanced water contact angle and droplet behavior.

Table 4. RMS surface roughness values estimated from the AFM images analysis for the Co-4 sample compared to the bare glass substrate.

Sample	RMS Surface Roughness (nm)
reference	0.7
Co/4-l	6.7
Co/4-m	6.8
Co/4-h	10.0

3.4. Mirror Silvering

After the hydrophilic coating fabrication on the front side of the glass tiles and its physicochemical characterization, the deposition of a mirror was performed on the backside

under a chemical route. In brief, this chemical approach, referred as the "Tollens' reaction", is a wet chemistry method, where the silver ions are reduced to metallic silver and deposited onto the glass surface. The alkaline environment facilitates the reduction of Ag^+ ions to Ag^0 in the presence of the reducing agent (glucose) [39]. The exact process involves mixing 7.5 mL of a 0.1 M aqueous $AgNO_3$ solution with an appropriate quantity of NH_3 and KOH solution (2.5 mL of 0.8 M) in order to produce $[Ag(NH_3)_2]^+$ ions. Next, this solution is mixed and agitated with 0.5 mL of 0.24 M glucose. The final solution is then injected on the backside of the glass. Gradually, the silver ions are reduced to metallic silver, following the next equation:

$$CH_2OH(CHOH)_4CHO + 2[Ag(NH_3)_2]^+ + 3OH^- \rightarrow 2Ag + CH_2OH(CHOH)_4COO^- + 4NH_3 + 2H_2O \quad (1)$$

3.5. Long-Term Stability and Cost Analysis for CSP Mirror Fabrication

To assess the long-term stability of the TiO_2 coating applied to the mirror glass tile using the Co/4-l sample, the tiles were exposed to outdoor conditions for a six-month span, during which its reflectivity was periodically monitored through angle measurements. This regular monitoring aimed to detect any potential changes in the coating's surface properties over time. By adopting this systematic approach, the study ensured a reliable and accurate evaluation of the coating's performance and provided insight into its ability to retain its functional properties under consistent environmental conditions. The results consistently presented near-zero percent alterations throughout the entire monitoring period, suggesting exceptional stability and resistance of the TiO_2 coating to degradation under prolonged conditions. Furthermore, these findings suggest that the coating not only has proven to be maintained over time but also acted as an efficient anti-soiling coating due to its superior water-attracting properties.

Moreover, an initial cost analysis was accomplished to estimate the feasibility of scaling up the process for real-word applications, specifically for CSP mirror fabrication. The fabrication of the TiO_2 coatings using the sol-gel method requires an annealing step above 400 °C, which can damage the CSP mirror.

To address this issue, the TiO_2 thin film should be deposited on one side of a bare glass tile, while the CSP mirror will be chemically deposited on the opposite side using a silvering process. This approach divides the overall cost into two distinct components: the expense of TiO_2 coating deposition and that of mirror fabrication. For the estimation of costs associated with the titania coatings and mirrors, the online catalog of a commercial chemical company [40] was used. Table 5 lists the prices and associated costs of the chemical reagents required for both the TiO_2 coatings and the silvering process. It should be emphasized that international developments have a significant impact on reagent prices and a stabilization of these prices is anticipated. In addition, high quantities of reagents were selected to reduce the estimated costs during scale-up. It is important to mention that the expenses for essential equipment and consumables (e.g., 50 L tank, annealing furnace, dip-coating system) are excluded from this calculation because: (i) these items will only need to be purchased once; and (ii) their costs will be distributed across the total number of CSP mirrors produced, becoming negligible when the technology transitions to industrial-scale manufacturing.

To fabricate hydrophilic coatings for lab-scale CSPs (4×4 cm^2 coated area), a minimum quantity of 91 mL for Co/4 titania precursor solution should be prepared by mixing ethanol, triton X-100, TTIP, and acetic acid, costing 4.68 € (as detailed in Table 6). This solution is sufficient for dipping multiple 16 cm^2 samples. Assuming ten dipping cycles with the same solution, the cost per hydrophilic coating is 0.47 € per glass tile. Including the 0.67 € cost for silvering the back side, the total preparation cost for each coated glass tile is 1.14 €.

Table 5. Chemical reagent costs for the TiO_2 coating and the silvering processes.

Reagent	Quantity (L or g)	Price (€)	Cost Per Unit (€/L or €/g)
ethanol	62.0	2980	48.06
triton X-100	2.5	189	75.60
TTIP	2.5	309	123.60
acetic acid	2.5	161	64.40
ammonia *	880	49.8	0.06
potassium hydroxide *	12,000	643	0.05
silver nitrate *	100	518	5.18
dextrose *	1000	250	0.25

* Quantity in g.

Table 6. Chemical reagent costs for the best TiO_2 coating and the silvering processes.

Reagent		16 cm^2 CSP		1 m^2 CSP	
	Cost Per Unit (€/L or €/g)	Quantity (L or g)	Total Cost (€)	Quantity (L or g)	Total Cost (€)
ethanol	48.06	0.082	3.94	45.055	2165.34
triton X-100	75.60	0.004	0.30	2.198	166.17
TTIP	123.60	0.002	0.25	1.099	135.84
acetic acid	64.40	0.003	0.19	1.648	106.13
precursor solution	-	**0.091**	**4.68**	**50**	**2573.48**
ammonia *	0.06	0.034	0.002	21.250	1.28
potassium hydroxide *	0.05	0.112	0.006	70.000	3.50
silver nitrate *	5.18	0.127	0.66	79.375	411.16
dextrose *	0.25	0.022	0.0055	13.750	3.44
precursor solution	-	**0.295**	**0.6735**	**184.375**	**419.38**

* Quantity in g. Bolded values represent the respective total quantities and costs for both precursor solutions.

For practical applications, CSP collectors require an active surface area of 1 m^2, which is 625 times larger than the lab-scale model. Scaling up to this size, a 50 L bath tank is needed to ensure full coverage with the titania precursor solution during the dip-coating process. As shown in Table 6, the required volumes result in a total cost of 2573.48 €, or 514.7 € per m^2 of coated glass (assuming the solution can be reused five times). Similarly, silvering process volume scales by a factor of 625, with a total cost of 419.4 € per mirror (Table 6). Therefore, the total manufacturing cost for a 1 m^2 CSP collector with a hydrophilic coating is 934.1 €.

This cost is fairly reasonable when considering the significant efficiency and durability benefits these coatings offer. Although it may appear high compared to the basic manufacturing costs of untreated glass, the added value from improved performance, such as increased solar reflectivity and potential self-cleaning properties, justifies the investment in high-performance CSP applications. Additionally, scalability and solution reuse reduce per-unit costs, making it a competitive choice over the long term for energy systems that emphasize efficiency and reduced maintenance expenses.

4. Conclusions

In this study, the development, characterization, and practical application of TiO_2 coatings on glass substrates were explored. A sol-gel dip-coating method was systematically employed to deposit TiO_2 films, followed by annealing to achieve the desired physicochemical properties. Parameters such as precursor concentration and withdrawal speed were carefully optimized to produce coatings with superior optical transparency, surface uniformity, and hydrophilicity. Characterization techniques, including UV/Vis spectroscopy, SEM, AFM, Raman, XPS, and contact angle measurements were utilized to

assess the effectiveness of the coatings and provide detailed insights into their structural, optical, and functional properties.

The experimental results revealed that uniform TiO_2 super-hydrophilic films can be successfully formed on glass substrates when the precursor reagent is dissolved in an ethanol-based solution and annealed at 550 °C. The developed TiO_2 coatings exhibited the chemical structure of anatase, minimal reflection losses, and super-hydrophilic behavior, as confirmed by the wettability measurements. Additionally, it was observed that slower withdrawal speeds and diluted precursor solutions yielded the most uniform and transparent coatings. These optimized parameters effectively reduced surface roughness and minimized optical transmittance losses, crucial for CSP mirror applications. The coatings also maintained their hydrophilic properties during long-term stability tests, confirming their durability and functional reliability.

A cost analysis of scaling up the coating and mirror fabrication processes demonstrated the economic viability of the technology for industrial applications. The production cost of a 1 m^2 CSP collector featuring a hydrophilic coating and a silvered mirror was estimated at 934.1 €. Although this is higher than the cost of untreated glass, it offers substantial value through enhanced performance and durability. The reuse of solutions and scalability of the process further contribute to its cost-effectiveness, reinforcing its potential for widespread adoption in CSP technologies aimed at increasing efficiency and reducing maintenance requirements.

In conclusion, this study underscores the promise of TiO_2 coatings as an innovative solution for CSP systems, integrating advanced material properties with practical manufacturability. The results provide a foundation for future research and large-scale industrial implementation, highlighting the essential balance between material optimization, deposition parameters, and cost-efficiency in achieving high-performance solar energy systems. By combining hydrophilic coatings with mirror fabrication, this study exemplifies a comprehensive approach to tackling energy and sustainability challenges. Continued research focused on enhancing durability, efficiency, and environmental impact—such as examining the film's stability and performance under various conditions to simulate real-life situations (e.g., humidity, degradation, mechanical abrasion, etc.) —will further establish the role of TiO_2 coatings in various high-performance applications, reinforcing their industrial-friendliness and practicality.

Author Contributions: Conceptualization, M.K.A., K.G. and P.F.; methodology, validation, M.K.A. and P.F.; investigation; G.V.T., M.K.A., N.M. and A.K.; writing—original draft preparation, G.V.T. and M.K.A.; writing—review and editing, C.M., K.G. and P.F.; supervision, C.M., K.G. and P.F.; project administration, resources, K.G. All authors have read and agreed to the published version of the manuscript.

Funding: This research was funded by the EC, within the EU Framework Programme for Research and Innovation Horizon 2020, grant number 786483.

Institutional Review Board Statement: Not applicable.

Informed Consent Statement: Not applicable.

Data Availability Statement: Data available on request from the authors.

Conflicts of Interest: The authors declare no conflicts of interest.

References

1. Afzal, A.; Habib, A.; Ulhasan, I.; Shahid, M.; Rehman, A. Antireflective self-cleaning TiO_2 coatings for solar energy harvesting applications. *Front. Mater.* **2021**, *8*, 687059. [CrossRef]

2. Zhou, C.; Xi, Z.; Stacchiola, D.J.; Liu, M. Application of ultrathin TiO_2 layers in solar energy conversion devices. *Energy Sci. Eng.* **2022**, *10*, 1614–1629. [CrossRef]
3. Hayali, A.; Alkaisi, M.M. High efficiency perovskite solar cells using DC sputtered compact TiO_2 electron transport layer. *EPJ Photovolt.* **2021**, *12*, 8. [CrossRef]
4. Hendi, A.A.; Alanazi, M.M.; Alharbi, W.; Ali, T.; Awad, M.A.; Ortashi, K.M.; Aldosari, H.; Alfaifi, F.S.; Qindeel, R.; Naz, G.; et al. Dye-sensitized solar cells constructed using titanium oxide nanoparticles and green dyes as photosensitizers. *J. King Saud Univ. Sci.* **2023**, *35*, 102555. [CrossRef]
5. Banerjee, S.; Dionysiou, D.D.; Pillai, S.C. Self-cleaning applications of TiO_2 by photo-induced hydrophilicity and photocatalysis. *Appl. Catal. B Environ.* **2015**, *176*, 396–428. [CrossRef]
6. Park, J.Y. How titanium dioxide cleans itself. *Science* **2018**, *361*, 753. [CrossRef]
7. Romanos, G.E.; Athanasekou, C.P.; Katsaros, F.K.; Kanellopoulos, N.K.; Dionysiou, D.D.; Likodimos, V.; Falaras, P. Double-side active TiO_2-modified nanofiltration membranes in continuous flow photocatalytic reactors for effective water purification. *J. Hazard. Mater.* **2012**, *211*, 304–316. [CrossRef]
8. Arfanis, M.K.; Adamou, P.; Moustakas, N.G.; Triantis, T.M.; Kontos, A.G.; Falaras, P. Photocatalytic degradation of salicylic acid and caffeine emerging contaminants using titania nanotubes. *Chem. Eng. J.* **2017**, *310*, 525–536. [CrossRef]
9. Arfanis, M.K.; Theodorakopoulos, G.V.; Anagnostopoulos, C.; Georgaki, I.; Karanasios, E.; Romanos, G.E.; Markellou, E.; Falaras, P. Photocatalytic removal of thiamethoxam and flonicamid pesticides present in agro-industrial water effluents. *Catalysts* **2023**, *13*, 516. [CrossRef]
10. Theodorakopoulos, G.V.; Arfanis, M.K.; Sánchez Pérez, J.A.; Agüera, A.; Cadena Aponte, F.X.; Markellou, E.; Romanos, G.E.; Falaras, P. Novel pilot-scale photocatalytic nanofiltration reactor for agricultural wastewater treatment. *Membranes* **2023**, *13*, 202. [CrossRef]
11. Momoli, R.; Giacomazzo, S.; Gandin, A.; Brusatin, G. Anti-fog nanocomposite coatings of enhanced durability. *J. Sol-Gel Sci. Technol.* **2022**, *101*, 46–57. [CrossRef]
12. Mishra, A.; Gill, F.S.; Bhatt, N.; Rathod, A.P.S.; Rajput, A. Fabrication of antireflective superhydrophobic coating for self-cleaning solar panels and study of energy efficiency. *Phys. Fluids* **2024**, *36*, 017111. [CrossRef]
13. Drelich, J.; Chibowski, E. Superhydrophilic and superwetting surfaces: Definition and mechanisms of control. *Langmuir* **2010**, *26*, 18621–18623. [CrossRef] [PubMed]
14. Patil, J.V.; Mali, S.S.; Hong, C.K.; Kim, J.H.; Patil, P.S. Structural, morphological, and wettability study of electrochemically anodized 1D TiO_2 nanotube arrays. *Appl. Phys. A* **2017**, *123*, 610. [CrossRef]
15. Vrakatseli, V.; Farsari, E.; Mataras, D. Wetting properties of transparent anatase/rutile mixed phase glancing angle magnetron sputtered nano-TiO_2 films. *Micromachines* **2020**, *11*, 616. [CrossRef]
16. Chakhtouna, H.; Benzeid, H.; Zari, N.; Qaiss, A.e.k.; Bouhfid, R. Recent progress on Ag/TiO_2 photocatalysts: Photocatalytic and bactericidal behaviors. *Environ. Sci. Pollut. Res.* **2021**, *28*, 44638–44666. [CrossRef]
17. Pawar, T.J.; López, D.C.; Romero, J.L.O.; Montesinos, J.V. Surface modification of titanium dioxide. *J. Mater. Sci.* **2023**, *58*, 6887–6930. [CrossRef]
18. Cedillo-González, E.I.; Hernández-López, J.M.; Ruiz-Valdés, J.J.; Barbieri, V.; Siligardi, C. Self-cleaning TiO_2 coatings for building materials: The influence of morphology and humidity in the stain removal performance. *Constr. Build. Mater.* **2020**, *237*, 117692. [CrossRef]
19. Wei, Y.; Wu, Q.; Meng, H.; Zhang, Y.; Cao, C. Recent advances in photocatalytic self-cleaning performances of TiO_2-based building materials. *RSC Adv.* **2023**, *13*, 20584–20597. [CrossRef]
20. Kontos, A.I.; Kontos, A.G.; Tsoukleris, D.S.; Vlachos, G.D.; Falaras, P. Superhydrophilicity and photocatalytic property of nanocrystalline titania sol–gel films. *Thin Solid Films* **2007**, *515*, 7370–7375. [CrossRef]
21. Zhao, W.; Jia, H.; Qu, J.; Yang, C.; Wang, Y.; Zhu, J.; Wu, H.; Liu, G. Sol-gel synthesis of TiO_2-SiO_2 hybrid films with tunable refractive index for broadband antireflective coatings covering the visible range. *J. Sol-Gel Sci. Technol.* **2023**, *107*, 105–121. [CrossRef]
22. Miki, H.; Akai, S.; Toyotama, A.; Okuzono, T.; Mata, J.; Yamanaka, J. Direct observation of light reflection by titania particles. *Chem. Lett.* **2024**, *53*, upad056. [CrossRef]
23. Wang, W.B.; Yanguas-Gil, A.; Yang, Y.; Kim, D.-Y.; Girolami, G.S.; Abelson, J.R. Chemical vapor deposition of TiO_2 thin films from a new halogen-free precursor. *J. Vac. Sci. Technol. A* **2014**, *32*, 061502. [CrossRef]
24. Kitano, M.; Funatsu, K.; Matsuoka, M.; Ueshima, M.; Anpo, M. Preparation of nitrogen-substituted TiO_2 thin film photocatalysts by the radio frequency magnetron sputtering deposition method and their photocatalytic reactivity under visible light irradiation. *J. Phys. Chem. B* **2006**, *110*, 25266–25272. [CrossRef]
25. Ghrairi, N.; Bouaicha, M. Structural, morphological, and optical properties of TiO_2 thin films synthesized by the electrophoretic deposition technique. *Nanoscale Res. Lett.* **2012**, *7*, 357. [CrossRef]

26. Wang, S.J.; Chang, W.-T.; Ciou, J.-Y.; Wei, M.-K.; Wong, M.S. Preparation of TiO_2 thin films by laser ablation for photocatalytic applications. *J. Vac. Sci. Technol. A* **2008**, *26*, 898–902. [CrossRef]
27. Zheng, L.; Cheng, H.; Liang, F.; Shu, S.; Tsang, C.K.; Li, H.; Lee, S.-T.; Li, Y.Y. Porous TiO_2 photonic band gap materials by anodization. *J. Phys. Chem. C* **2012**, *116*, 5509–5515. [CrossRef]
28. Cheng, X.; Hu, S.; Zeng, P.; Kuang, T.; Xie, G.; Gao, F. Structure and properties of TiO_2 films prepared by ion beam assisted deposition. *Surf. Coat. Technol.* **2007**, *201*, 5552–5555. [CrossRef]
29. Miyata, T.; Tsukada, S.; Minami, T. Preparation of anatase TiO_2 thin films by vacuum arc plasma evaporation. *Thin Solid Films* **2006**, *496*, 136–140. [CrossRef]
30. Tsoukleris, D.S.; Kontos, A.I.; Aloupogiannis, P.; Falaras, P. Photocatalytic properties of screen-printed titania. *Catal. Today* **2007**, *124*, 110–117. [CrossRef]
31. Manickam, K.; Muthusamy, V.; Manickam, S.; Senthil, T.S.; Periyasamy, G.; Shanmugam, S. Effect of annealing temperature on structural, morphological and optical properties of nanocrystalline TiO_2 thin films synthesized by sol–gel dip coating method. *Mater. Today Proc.* **2020**, *23*, 68–72. [CrossRef]
32. Bhandarkar, S.A.; Prathvi; Kompa, A.; Murari, M.S.; Kekuda, D.; Mohan, R.K. Investigation of structural and optical properties of spin coated TiO_2:Mn thin films. *Opt. Mater.* **2021**, *118*, 111254. [CrossRef]
33. Xu, Q.-c.; Wellia, D.V.; Sk, M.A.; Lim, K.H.; Loo, J.S.C.; Liao, D.W.; Amal, R.; Tan, T.T.Y. Transparent visible light activated C–N–F-codoped TiO_2 films for self-cleaning applications. *J. Photochem. Photobiol. A Chem.* **2010**, *210*, 181–187. [CrossRef]
34. Hornschuh, M.; Zwicker, P.; Schmidt, T.; Finke, B.; Kramer, A.; Müller, G. Poly (hexamethylene biguanide), adsorbed onto Ti-Al-V alloys, kills slime-producing *Staphylococci* and *Pseudomonas aeruginosa* without inhibiting SaOs-2 cell differentiation. *J. Biomed. Mater. Res.* **2020**, *108B*, 1801–1813. [CrossRef]
35. Antoniadou, M.; Sfaelou, S.; Lianos, P. Quantum dot sensitized titania for photo-fuel-cell and for water splitting operation in the presence of sacrificial agents. *J. Chem. Eng.* **2014**, *254*, 245–251. [CrossRef]
36. Balis, N.; Dracopoulos, V.; Stathatos, E.; Boukos, N.; Lianos, P. A solid-state hybrid solar cell made of nc-TiO_2, CdS quantum dots, and P3HT with 2-Amino-1-methylbenzimidazole as an interface modifier. *J. Phys. Chem. C* **2011**, *115*, 10911–10916. [CrossRef]
37. Biesinger, M.C.; Lau, L.W.M.; Gerson, A.R.; Smart, R.S.C. Resolving surface chemical states in XPS analysis of first row transition metals, oxides and hydroxides: Sc, Ti, V, Cu and Zn. *Appl. Surf. Sci.* **2010**, *257*, 887–898. [CrossRef]
38. Peng, W.-C.; Chen, Y.-C.; He, J.-L.; Ou, S.-L.; Horng, R.-H.; Wuu, D.-S. Tunability of p- and n-channel TiO_x thin film transistors. *Sci. Rep.* **2018**, *8*, 9255. [CrossRef]
39. Panneerselvam, R.; Xiao, L.; Waites, K.B.; Atkinson, T.P.; Dluhy, R.A. A rapid and simple chemical method for the preparation of Ag colloids for surface-enhanced Raman spectroscopy using the Ag mirror reaction. *Vib. Spectrosc.* **2018**, *98*, 1–7. [CrossRef]
40. Sigma-Aldrich Products. Available online: https://www.sigmaaldrich.com (accessed on 22 November 2024).